Blockage of natural convection boundary layer flow in a multizone enclosure

Douglas Scott*
Department of Mechanical Engineering, Clemson University, Clemson, SC, USA

Ren Anderson†
Thermal Research Branch, Solar Energy Research Institute, Golden, CO, USA

Richard Figliola‡
Department of Mechanical Engineering, Clemson University, Clemson, SC, USA

Two separate mechanisms can be responsible for natural convection flow between the hot and cold zones of a multizone enclosure: (1) bulk density differences created by temperature differences between the fluid in the hot and cold zones (bulk-density-driven flow) and, (2) thermosyphon "pumping" generated by boundary layers or plumes (motion-pressure-driven flow). This paper reports the results of an experimental study that examines the transition between flow regimes, as a function of aperture size, in a two-zone enclosure with heated and cooled end walls. A constant heat flux boundary condition was maintained on one vertical end wall, and an isothermal cold temperature sink was maintained on the opposite vertical end wall. All of the remaining surfaces were highly insulated. The transition between the boundary-layer-driven regime and the bulk-density-driven regime was established as a function of the geometry of the aperture in a partition that separated the hot and cold zones. The results of the study demonstrate that transition from the boundary-layer-driven regime to the bulk-density-driven regime is caused by blockage of the boundary layer flow when the area of the flow aperture is reduced below a critical value. A preliminary model has been developed which predicts that the critical aperture area for the onset of flow blockage is directly proportional to the number of active heat transfer surfaces and inversely proportional to the Rayleigh number which characterizes the level of heating and cooling provided to the active heat transfer surfaces.

Keywords: natural convection; aperture flow; boundary layer flow; air flow

Introduction

There has been a strong interest in the behavior of natural convection in enclosures because of the important role that it plays in determining the performance of thermal insulation systems, solar collectors, thermal storage systems, building space conditioning systems, and smoke and fire spread in buildings. Recent reviews on the topic of natural convection in enclosure geometries have been prepared by Catton[1], Ostrach[2], and Churchill[3]. Reviews of research directly related to smoke and fire spread in buildings have been given by Quintiere[4] and by Yang and Lloyd[5].

In many of the applications cited above, the convective heat transfer process is complicated by the presence of internal partitions. There are two primary mechanisms that can drive natural convection flow through apertures in multizone enclosures: (1) bulk density differences between hot and cold zones, and (2) motion pressure differences generated by natural convection boundary layers or plumes. The terminology "motion pressure" refers to pressure differences generated by fluid motion above and beyond hydrostatic pressure differences.

Figure 1 illustrates the differences between the two mechanisms. The flow system under study is closed, recirculating, and divided by a partition with an aperture of width w and height h. The bulk density regime (Figure 1(a)) is characterized by fluid temperatures, T_C and T_H, measured at points remote from the partition. T_C and T_H result in differing bulk densities of ρ_C and ρ_H and differing hydrostatic pressure fields between zones. Because the flow is always recirculating, there must exist at some height h' a level of no flow (horizontally) and, therefore, a zero pressure difference between the two zones. It is easily shown that the pressure difference (left to right) above and below h' is $(\rho_H - \rho_C)gz$, where z is measured from h'. The resulting velocity profile for such conditions has been previously examined by Brown and Solvason[6].

The boundary layer regime (Figure 1(b)) is characterized by wall temperatures, T'_C and T'_H, and fluid temperatures. T_C and T_H. In this case, though, the midzone temperatures T_H and T_C are approximately equal and approach some median temperature between T'_C and T'_H. The density throughout both zones is relatively uniform, and no hydrostatic pressure differences arise. The temperature difference between the fluid and the walls results in the formation of boundary layers which drive convective heat transfer between the hot and cold walls. Transition from a motion pressure to a bulk-density-driven regime can occur if, for a given aperture size, $T_H - T_C$ is increased so that T_C and T_H begin to differ significantly or if, for a given wall temperature difference, the size of the aperture is constricted so that normal boundary layer flow begins to be blocked.

* Graduate Research Assistant
† Engineer
‡ Associate Professor

Researchers who have examined smoke and fire spread in buildings have long recognized the existence of two types of flow behavior, depending on whether the flow aperture is large or small[7]. Satoh, Lloyd, and Yang[8] have conducted numerical calculations that span the range from the "small opening limit" to the "large opening limit" for a cubic enclosure with a gas burner located centrally on the floor of the enclosure.

Brown and Solvason[6] conducted heat transfer measurements of bulk-density-driven flow in an air-filled enclosure that was divided into hot and cold regions by a single partition with a centrally located rectangular opening. Using inviscid calculations and assuming isothermal fluid reservoirs on either side of the partition, they demonstrated that the heat transfer through the partition could be correlated by the relationship

$$Nu = (C/3)^{2/3} A_W^{2/3} A_H (Ra^* Pr)^{1/3} \qquad (1)$$

The constant C is the discharge coefficient for the aperture, and as reported by Brown and Solvason, lies in the range $0.6 \leqslant C \leqslant 0.98$.

The Nusselt number Nu in Equation 1 is based upon the temperature difference $\Delta T = T_H - T_C$ between the fluid reservoirs on either side of the partition at the midheight of the aperture. Bulk density flow models similar to Equation 1 have been used as the basis for analyzing airflow in solar buildings[9,10].

Multizone flows driven by natural convection boundary layers have been studied by several investigators. Two-dimensional apertures have been considered by Jankowski, Ward, and Probert[11], Bejan and Rossie[12], Nansteel and Greif[13], Bajorek and Lloyd[14], Chang, Lloyd, and Yang[15], and Lin and Bejan[16]. All of these studies were experimental, with the exception of that of Chang, Lloyd and Yang, which was a finite difference model of a geometry similar to the experimental work of Bajorek and Lloyd.

Chang, Lloyd, and Yang[15] considered partitions that extended equal distances from the floor and ceiling of a square cavity, and calculated the reduction in heat transfer that occurred as the height of the partitions was increased. Lin and Bejan provided a perturbation solution valid in the limit Ra → 0, in addition to their experimental results.

Nansteel and Greif[13] and Lin and Bejan[16] conducted experiments at large Rayleigh numbers and demonstrated that the presence of a partition between zones tends to damp out the natural convection boundary layer flow in subregions that are subjected to stable thermal boundary conditions. This effect reduces the wall area exposed to the primary boundary layer flow and results in an overall reduction in the convective heat transfer between the hot and cold surfaces on either side of the partition. Nansteel and Greif[17] correlated their data to include this effect. Their correlation, expressed in terms of the present notation, is

$$Nu' = 0.929 A_H^{0.332} Ra^{*0.172} \qquad (2)$$

$$1/4 \leqslant A_H \leqslant 1 \qquad (3)$$

$$A_W \geqslant 0.093 \qquad (4)$$

where Nu' is based on the temperature difference $\Delta T' = T'_H - T'_C$ between the hot and cold end walls.

The only previous three-dimensional study of natural convection through an aperture in the boundary layer regime is that of Nansteel and Greif[17], who considered a partition with a variable-width opening. They compared their three-dimensional results to their previous study with $A_W = 1.0$ (Nansteel and Greif[13]) and found that the heat transfer between zones did not strongly depend on the width of the aperture for $A_W \geqslant 0.093$.

A comparison between Equation 1 and Equation 2 demonstrates that the natural convection flow regime that governs the

Notation

A	area
A_H	Aperture height ratio, h/H
A_S	Aspect ratio, H/L
A_W	Aperture width ratio, w/W
C	Discharge coefficient for aperture
c_p	Specific heat at constant pressure
g	Acceleration due to gravity
h	Height of aperture (y-dimension)
H	Height of test cell/partition (y-dimension)
k	Thermal conductivity
L	Length of test cell (x-dimension)
Nu	Nusselt number, $q''H/k\Delta T$
Nu'	Nusselt number, $q''H/k\Delta T'$
$\overline{Nu}$	Average Nusselt number, $\dfrac{1}{H}\displaystyle\int_0^H Nu(y)\,dy$
P	Hydrostatic pressure
Pr	Prandtl number, $\mu c_p/k$
q''	Average heat flux per unit area
q	Total heat flux, $q''A$
Ra^*	Flux-modified Rayleigh number, $g\beta H^4 q''/v\alpha k$
$\Delta T'$	Temperature difference measured between points located at xyz coordinates $(0, H/2, W/2)$ and $(L, H/2, W/2)$ (the midpoints of the hot and cold walls)
ΔT	Temperature difference measured between points located at xyz coordinates $(L/4, h/2, W/2)$ and $(3L/4, h/2, W/2)$ (a difference in the characteristic zone temperatures at an elevation of aperture midheight)
w	Width of aperture (z-dimension)
W	Width of test cell/partition (z-dimension)
x, y, z	Nondimensional, spatial coordinates, X/L, Y/H, Z/W

Greek

α	Thermal diffusivity, $k/\rho c_p$
β	Coefficient of thermal expansion
ρ	Density
v	Kinematic viscosity, μ/ρ
μ	Viscosity
δ	Boundary layer thickness
θ	$(T - T_C)/(T' - T_C)$
θ^*	$\Delta T/\Delta T'$

Superscript

'	Midpoint

Subscripts

bl	Boundary layer
C	Cold zone
H	Hot zone

(a)

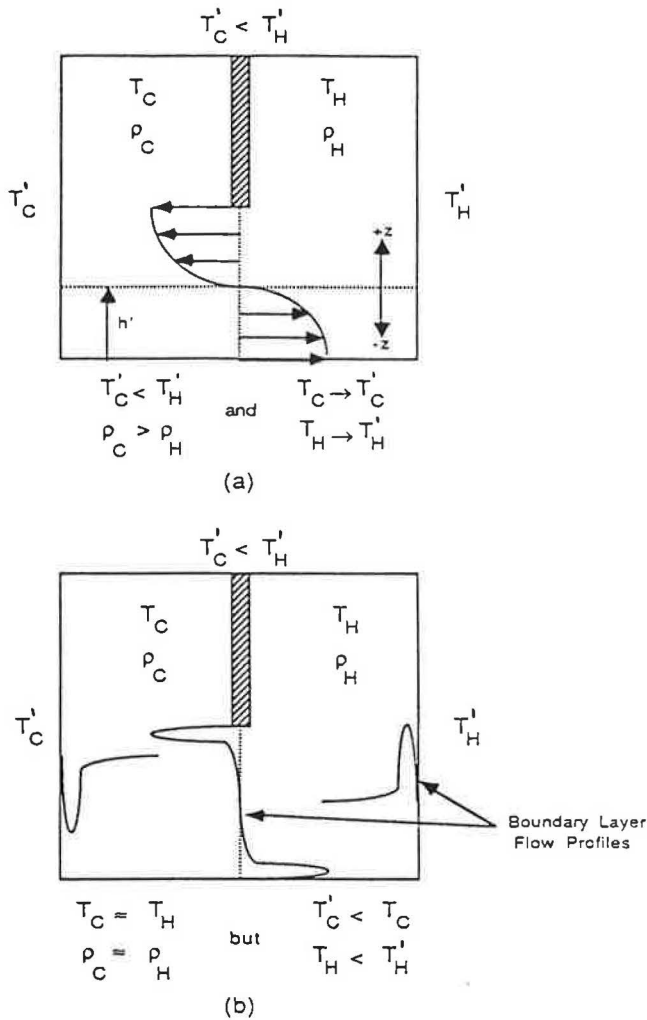

Boundary Layer
Flow Profiles

(b)

Figure 1 Typical (a) bulk density and (b) motion pressure heat transfer regimes

flow through the aperture has a strong impact upon the geometric dependence of the heat transfer coefficient. In the bulk-density-driven regime (Equation 1), the heat transfer between zones depends strongly on both the aperture height ratio A_H and the aperture width ratio A_W. In the motion pressure regime (Equation 2) the heat transfer between zones depends weakly on the aperture height ratio and appears to be independent of the aperture width ratio. Because of these differences, it is important to be able to predict the nature of a multizone flow. Our primary objective is to determine the transition between the bulk-density- and motion-pressure-driven regimes as a function of aperture geometry in a simple two-zone enclosure with heated and cooled end walls.

Isothermality factor

The isothermality factor θ^* is defined for this study as

$$\theta^* = \Delta T/\Delta T' \tag{5}$$

where ΔT is the bulk temperature difference and $\Delta T'$ is the end wall temperature difference. The significance of θ^* can be inferred by examining its limits. As θ^* approaches 0, ΔT becomes very small compared with $\Delta T'$, indicating relatively little bulk density difference between the two zones. For small

θ^*, therefore, heat transfer occurs primarily by boundary layer flow. As θ^* approaches 1, the hot and cold zones approach isothermal states close in temperature to their respective end walls (hence the name "isothermality factor"). The resulting relative increase in ΔT produces bulk density differences between zones, causing bulk-density-driven flows.

Boundary layer flow blockage model

Nansteel and Greif[17] have demonstrated that heat transfer between two zones in the boundary layer regime is nearly independent of the width of the aperture between zones for $A_W \geqslant 0.093$ and $0.25 \leqslant A_H \leqslant 1.0$. However, as the width of the aperture is reduced below values considered by Nansteel and Greif, the boundary layer flow will eventually be blocked. Flow blockage will result in the formation of large temperature differences across the aperture and will cause a transition from motion-pressure- to bulk-density-driven convection.

The structure of the horizontal boundary layers near the top and bottom surfaces of an enclosure with differentially heated end walls are not well understood, even for the relatively simple case of an enclosure without partitions[18]. However, the onset of boundary layer flow blockage can be estimated by applying a continuity argument to the flow in the vertical boundary layers and the flow through the aperture. If the area of the aperture is smaller than the area required by the boundary layer flow, then the flow will have to accelerate to pass through the aperture. The additional driving force required to convect the flow through the aperture can be provided only by the creation of bulk density differences between the hot and cold zones of the enclosure.

The flow area required by the boundary layers on heated and cooled surfaces can be estimated by calculating the product of the thickness and width of the vertical boundary layer, where

$$A_{bl} = W\delta \tag{6}$$

According to the flow continuity criteria described above, flow blockage will occur when

$$A_{bl}/hw = W\delta/hw \sim 1 \tag{7}$$

For laminar flow it can be shown that the natural convection boundary layer thickness next to a vertical surface is scaled by the relationship[19]

$$\delta/H \sim 1/Ra^{*1/5} \tag{8}$$

If we assume that the height, width, and average heat flux from each active surface are H, W, and q'', then the flow blockage criteria expressed by Equation 6 can be arranged into the simple form

$$A_W A_H \sim 1/Ra^{*1/5} \tag{9}$$

The left side of Equation 9 is the ratio of the area of the aperture to the cross-sectional area of the enclosure. Equation 9 predicts that the onset of flow blockage is inversely proportional to the Rayleigh number which characterizes the natural convection flow.

Experimental apparatus and procedure

The experimental measurements were performed in an approximately cubic water-filled test cell with $L = 56.5$ cm, $H = 58.4$ cm, and $W = 57.2$ cm (Figujre 2). Two opposing vertical walls and the cell bottom were constructed of nickel-plated aluminum 1.27 cm thick. The remaining vertical walls were constructed of plate glass 0.64 cm thick. The top of the cell was constructed of Plexiglass 2.54 cm thick. A constant heat flux
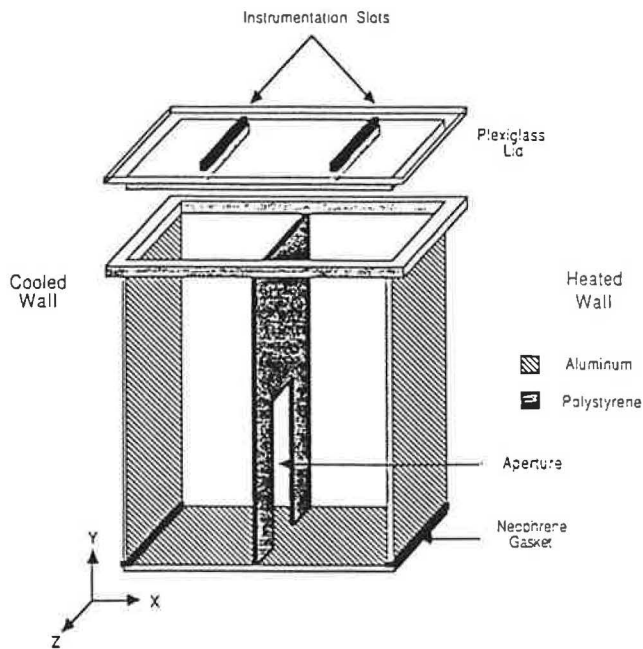
Instrumentation Slots

Figure 2 Schematic of test cell and partition

boundary condition was maintained on one vertical aluminum wall, and an isothermal temperature sink was maintained on the opposite vertical aluminum wall. All other boundaries were highly insulated, producing nearly adiabatic boundary conditions.

All fluid properties used in the calculation of nondimensional quantities were evaluated at the average of the midpoint temperature of the hot and cold walls. A neoprene gasket of 0.32 cm thickness separated the vertical aluminum walls from the floor of the test cell. The vertical dividing partition was constructed of Styrofoam 2.54 cm thick, 58.4 cm high, and 57.2 cm wide. A half-height rectangular aperture was cut into the middle of the partition (Figure 2). The width of the aperture was increased with each test from 0.32 cm until it extended across the entire width of the test cell. Tests were also conducted without an aperture in the partition and with the partition completely removed from the test cell.

The constant-heat-flux boundary condition on the heated wall was maintained with 16 electric-resistance zone heaters wired in parallel and attached to the outside of the heated aluminum wall. Power input to the heaters was monitored by wattmeters calibrated to within $\pm 5\%$. The temperature variations on the cold wall were kept to within 3% of the end-to-end temperature difference $\Delta T'$ by circulating chilled water through two zones of channels milled into a 2.54-cm Plexiglass plate bolted to the back of the aluminum wall.

To reduce heat loss through the cell walls, the test cell was insulated with 5.1 cm of Styrofoam insulation and 15.2 cm of fiberglass batting. The heat loss from the test cell was measured to be 2.2 W/°C temperature difference between the average test cell temperature and the ambient. All tests were conducted keeping the average temperature of the test cell as close as possible to the ambient temperature to minimize losses. The power input to the test cell was varied between 50 and 600 W. Heat losses from the test cell were calculated from the measured core temperature distribution and the measured heat loss characteristics of the test cell. The heat loss from the test cell was generally less than 5% of the end-to-end heat transfer and was subtracted from the power input to the test cell when the data

were analyzed. The conductance of the partition was measured in the absence of an aperture and found to be 0.5 W/°C temperature difference between the fluid on either side of the partition. Conduction through the partition was generally less than 1% of the total end-to-end heat transfer in the test cell.

Temperatures were measured in the hot wall, the cold wall, and in the floor of the test cell by thermocouples buried 0.16 cm from the inside wall surface and located along the vertical axis at $z = W/2$. Additional measurements were made at other z-locations on the vertical end walls to ensure that temperature did not vary in the z-direction. Two thermocouple rakes were used to measure temperature simultaneously at nine vertical locations at the midpoint of the hot and cold zones on either side of the partition. The amount of heat conduction in the floor of the test cell was found to be less than 1% of the total end-to-end transfer.

The temperature and the power input to the heaters were measured with a microcomputer-based data acquisition system. An ice-point reference was used to correct for any drift in the calibration of the temperature measurement channels on the data acquisition system. The experimental error associated with temperature measurements using this system is estimated to be $\pm 0.2°C$. Power input, wall temperature, and rake temperature were taken every 2 min and displayed graphically on the computer monitor. Generally, it took about 10 h for the test cell to reach steady state when the power setting or the aperture geometry was changed. Steady state was defined as no detectable trend in temperature or power level over the cells entire displayed histories. Resolution of the monitor made trends of $\pm 0.3°C$ and ± 4 W over 3 h detectable. After steady state had been reached, five sets of data were taken over a period of about 10 min and averaged to give the final data point for each power setting and aperture width ratio.

The major sources of experimental error are summarized in Table 1. These errors correspond to a 6% error in determination of the Nusselt number and nondimensional temperatures that are reported in the results.

Experimental results

Figure 3 shows the nondimensional temperature θ plotted as a function of the vertical (y) coordinate at two locations: (1) in the middle of the hot zone ($x = L/4$, $z = W/2$) (Figure 3(a)), and (2) in the middle of the cold zone ($x = 3L/4$, $z = W/2$) (Figure 3(b)). The nondimensional temperature θ is defined to be the difference between the local temperature and the cold-wall temperature divided by the difference between the midpoint temperature ($w = W/2$, $y = H/2$) and the cold wall.

Figure 3(a) demonstrates the dramatic increase in temperature that occurs in the upper portion of the hot zone when a half-height partition is present, acting as a trap for warm, buoyant fluid. This temperature increase results from a reduction of the strength of the boundary layer flow in the stable stratified region bounded by the top of the test cell, the upper half of the partition, and the upper half of the heated wall. Dye injection studies confirmed the presence of a large slowly rotating cell in this region. The formation of the cell has been

Table 1 Experimental uncertainties (95% confidence)

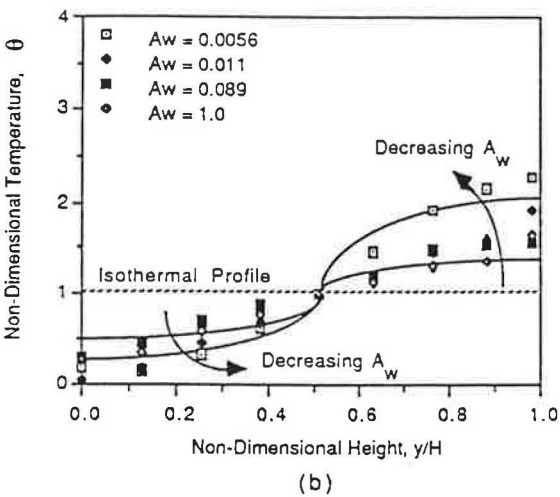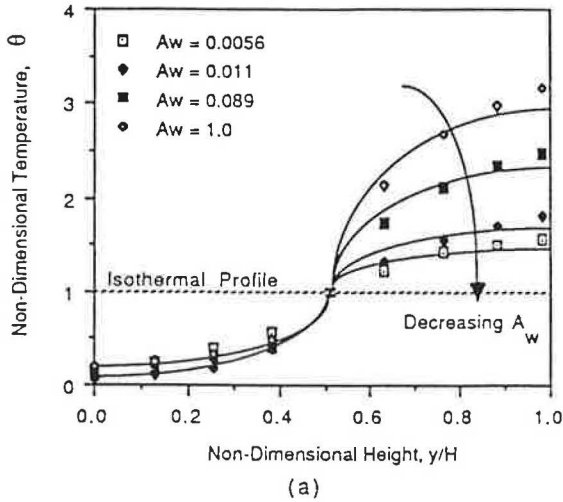|	
Temperature	$\pm 0.2°C$
Conduction in floor and partition	2%
Temperature difference	$\pm 2\%$
Power input	± 4 W
	(or $\pm 5\%$)

(a)

(b)

Figure 3 Dimensionless temperature θ as a function of vertical location: (a) hot zone; (b) cold zone

described previously by Lin and Bejan[16] and by Nansteel and Greif[17]. As the width of the aperture between the hot and cold zones is reduced, the temperature profiles in Figure 3(a) indicate that the level of thermal stratification in the hot zone is gradually reduced. As the boundary layer flow is blocked, the hot zone tends to become more isothermal and approaches the temperature of the hot end wall.

The cold-zone temperature profiles (Figure 3(b)) exhibit increased stratification as the aperture width is reduced. The magnitude of the stratification in the cold zone is determined by the temperature of the fluid exiting the hot zone. Because of the constant-flux boundary condition in the hot zone, the hot-zone temperature, and thus the cold-zone stratification, is inversely proportional to the size of the aperture.

Figure 4 examines the isothermality factor θ^* as a function of Ra*. When the size of the aperture is reduced, the fluid temperature difference between the hot and cold zones rapidly approaches the temperature difference between the hot and cold end walls. θ^* decreases as the Rayleigh number increases, indicating that high Rayleigh number flows are less likely to be blocked than small Rayleigh number flows, in qualitative agreement with the trend predicted by Equation 9.

Figure 5 illustrates the increase of the isothermality factor θ^* with the decrease of the width aperture ratio. The plot was generated from the correlations of the data in Figure 4. The

flatness in the curves indicates the region of independence from aperture size. Earlier boundary layer studies that concluded that heat transfer was largely independent of aperture width[13,17] were probably performed in this area. Recalling the definition of the isothermality factor, we clearly see that as the aperture size decreases the zone bulk temperature difference begins to become significant, and that transition from motion-pressure- to bulk-density-driven heat transfer eventually occurs. A possible area of transition is suggested by the points added from the simple blockage model of Equation 9.

In Figure 6, the zone-to-zone temperature difference ΔT measured during the experiment is compared to the zone-to-zone temperature difference for a bulk-density-driven flow, as calculated from Equation 1. The data and calculation shown in Figure 6 are for a constant zone-to-zone convective energy transfer of 500 W.

As the size of the flow aperture between zones is reduced, the bulk density flow model (Equation 1) predicts that the temperature difference required to transfer a given amount of heat across the aperture will have to increase steadily. However, the experimental observations indicate that the temperature difference between zones does not increase until a critical
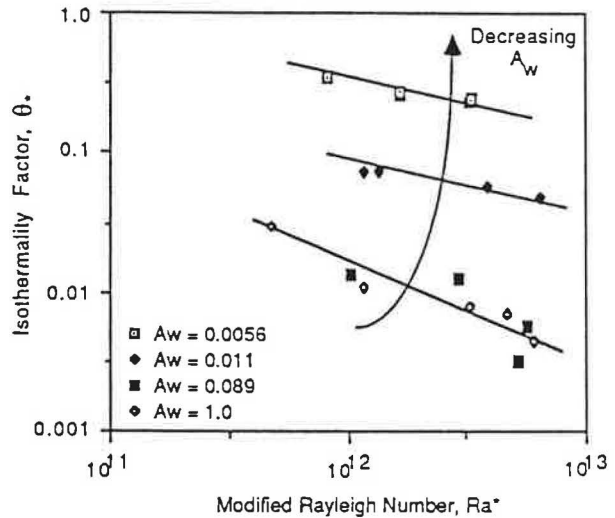

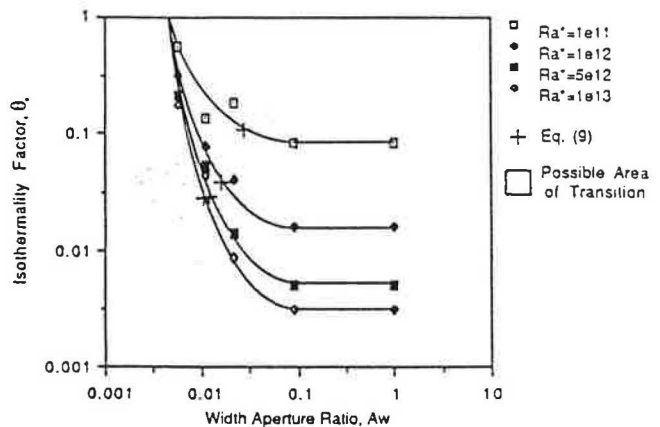*Figure 4* Isothermality factor θ^* as affected by modified Rayleigh number Ra*

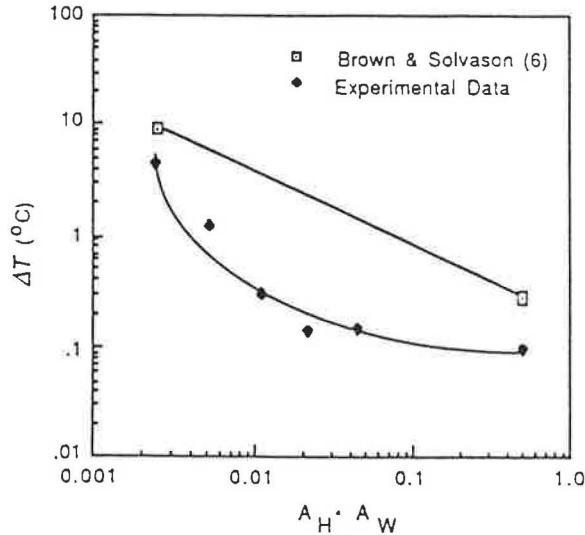*Figure 5* Isothermality factor θ^* as affected by width aperture ratio A_W

Figure 6 Comparison between temperature differences predicted by the bulk density flow model and experimental results

Figure 7 Nusselt number correlations

aperture area is reached. This critical aperture area is approximately 2% of the total cross-sectional area of the test cell. This result demonstrates that boundary layer "pumping" can have a significant impact upon the transport of fluid between hot and cold zones. The boundary layers can transport fluid through the aperture without requiring a large zone-to-zone temperature difference, provided that the aperture area is larger than the critical value for the onset of flow blockage.

Average Nusselt numbers are plotted as a function of Ra* in Figure 7. The heat transfer results, when the partition is completely removed from the test cell ($A_H = 1$), are shown in addition to data for $A_H = 0.5$ and variable values of A_W. Selected results from Nansteel and Greif[17] are plotted in Figure 7 for $A_H = .5$ (Equation 2). There is a dramatic drop in the average Nusselt number when A_H is decreased from 1 to 0.5 because of the relatively static pocket of hot fluid that is trapped in the upper half of the hot zone of the test cell. This trapped hot fluid inhibits heat transfer from the upper half of the hot wall.

Figure 7 demonstrates that when A_W is reduced, the heat transfer between the hot and cold end walls is also reduced. Least squares fits to the experimental data in Figure 7 produce the following correlations:

$$\overline{Nu} = 0.32Ra^{*0.21}, \quad A_H = 1.0, \quad A_W = 1.0 \tag{10}$$

$$\overline{Nu} = 0.20Ra^{*0.21}, \quad A_H = 0.5, \quad A_W = 1.0 \tag{11}$$

$$\overline{Nu} = 0.030Ra^{*0.27}, \quad A_H = 0.5, \quad A_W = 0.087 \tag{12}$$

$$\overline{Nu} = 0.003Ra^{*0.35}, \quad A_H = 0.5, \quad A_W = 0.0056 \tag{13}$$

In addition to an overall reduction in heat transfer (a trend consistent with behavior predicted by Equation 1 and Equation 2), there is an increase in the slope of the correlations, from 0.21 to 0.35, as the aperture width ratio A_W is decreased. The theoretical slope of the global correlation for a laminar natural convection boundary layer next to a constant-flux surface is $\frac{1}{5}$, and the slope predicted by the theoretical expression of Brown and Solvason for a bulk-density-driven flow is $\frac{1}{3}$.

Conclusions

Experimental measurements have been conducted to determine the onset of blockage of a natural convection boundary layer
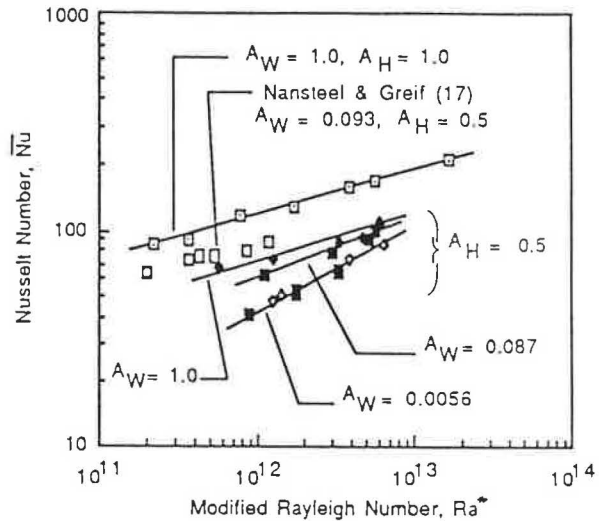
flow through a variable-size aperture in a simple two-zone enclosure. The height of the aperture between zones was held constant at half the overall height of the enclosure while the width ratio of the aperture was varied over the range $1 \geqslant A_W \geqslant 0.0056$. The natural convection flow was driven by heating and cooling the end walls of the enclosure. Blockage of the boundary layer flow through the aperture was found to occur when the area of the aperture was reduced below a critical area which was approximately 2% of the total cross-sectional area of the test cell.

Blockage of the boundary layer flow caused a reduction in the level of thermal stratification in the hot zone, increased the thermal stratification in the cold zone, increased the temperature difference between the hot and cold zones, and reduced the convective heat transfer between the hot and cold end walls. The increase in the temperature difference between the hot and cold zones caused the aperture flow to change from a regime driven primarily by the boundary layers on the hot and cold walls to a regime driven, in addition, by the density differences between the two zones.

A new parameter, the isothermality factor θ^* has been introduced to assist in detecting boundary layer flow blockage. A model that predicts the onset of blockages of the boundary layer flow has been developed and shown to describe the major features of the blockage phenomenon. This study demonstrates that boundary layers can be used to transport energy without large bulk fluid temperature differences, provided that the flow aperture area is larger than the critical value for the onset of flow blockage. This result has important implications for the design of flow apertures in solar buildings and other applications that rely upon natural convection to transport energy between zones in multizone enclosures.

References

1 Catton, I. Natural convection in enclosures, *6th Int. Heat Transfer Conf.*, National Research Council of Canada, Toronto, 1978

2 Ostrach, S. Natural convection heat transfer in cavities and cells. *7th Int. Heat Transfer Conf.*, Munich, Germany, 1982

3 Churchill, S. W. Free convection in layers and enclosures. In *Heat Exchanger Design Handbook*, ed. E. U. Schlunder. Hemisphere, Washington, D.C., 1983

4 Quintiere, J. Growth of fire in building compartments. In *Fire Standards and Safety*, ASTM STP 614, ed. A. F. Robertson. American Society for Testing and Materials, 1977, pp. 131–167

5 Yang, K. T. and Lloyd, J. R. Turbulent flow in vented simple and complex enclosures. In *Natural Convection: Fundamentals and Applications*, eds. S. Kakac, W. Aung, R. Viskanta. Hemisphere, Washington, D.C., 1985, pp. 303–329

6 Brown, W. G. and Solvason, K. R. Natural convection through rectangular openings in partitions. I. *Int. J. Heat Mass Transfer* 1962, **5**, 859–868

7 Thomas, P. H., Heselden, J. M., and Law, J. Fully-developed compartment fires: two kinds of behaviors. Fire Research Technical Paper no. 18, Fire Research Station, Borehamwood, England, 1967

8 Satoh, K., Lloyd, J. R., and Yang, K. T. Turbulent buoyant flow and smoke layers in a two-dimensional rectangular compartment with vertical vents. *Proc. 1980 Fall Meeting Eastern Section Combustion Inst.*, paper #22, 1980. See also K. Satoh, Experimental and finite difference study of dynamic fire behaviours in a cubic enclosure with a doorway. Report of Fire Research Institute of Japan, no. 55, 1983, pp. 17–29

9 Balcomb, J. D., Jones, G. F., and Yamaguchi, K. Natural convection airflow measurement and theory. *Ninth National Passive Solar Conf.*, Columbus, Ohio, 1984. See also G. F. Jones, J. D. Balcomb, and D. R. Otis, A model for thermally driven heat and air transport in passive solar buildings. ASME 85-WA/HT-69, 1985

10 Kirkpatrick, A., Hill, D., and Burns, P. Interzonal natural and forced convection heat transfer in a passive solar building. *ASME J. Solar Energy Eng.* to appear

11 Jankowski, H. E., Ward, J., and Probert, S. D. Free convection in vertical air-filled rectangular cavities filled with baffles. *6th Int. Heat Transfer Conf.*, Toronto, 1978

12 Bejan, A. and Rossie, A. N. Natural convection in undivided and partially divided rectangular enclosures. *J. Heat Transfer* 1981, **103**, 623–629

13 Nansteel, M. W. and Greif, R. Natural convection in undivided and partially divided rectangular enclosures. *J. Heat Transfer* 1982, **104**, 527–532

14 Bajorek, S. M. and Lloyd, J. R. Experimental investigation of natural convection in partitioned enclosures. *J. Heat Transfer* 1982, **104**, 527–532

15 Chang, L. C., Lloyd, J. R., and Yang, K. T. A finite difference study of natural convection in complex enclosures. *7th Int. Heat Transfer Conf.*, Munich, Germany, 1982

16 Lin, N. N. and Bejan, A. Natural convection in a partially divided enclosure. *Int. J. Heat Mass Transfer* 1983, **26**, 1867–1878

17 Nansteel, M. W. and Greif, R. An investigation of natural convection in enclosures with two- and three-dimensional partitions. *Int. J. Heat Mass Transfer* 1984, **27**, 561–571

18 Blythe, P. A., Daniels, P. G., and Simpkins, P. G. Thermal convection in a cavity: the core structure near the horizontal boundaries. *Proc. R. Soc. Lond. A*, 1983, **387**, 367–388

19 Bejan, A. The basic scales of natural convection heat and mass transfer in fluids and fluid-saturated porous media. *Int. Comm. Heat Mass Transfer* 1987, **14**, 107–123